ACS Photonics

Article

Cite This: ACS Photonics 2018, 5, 1794−1799

Multifunctional Light Sword Metasurface Lens

Zhengren Zhang,[†,‡,§] Dandan Wen,[†,§] Chunmei Zhang,[†] Ming Chen,[∥] Wei Wang,[†] Shuqi Chen,[⊥] and Xianzhong Chen*[,†]

[†]SUPA, Institute of Photonics and Quantum Sciences, School of Engineering and Physical Sciences, Heriot-Watt University, Edinburgh, EH14 4AS, United Kingdom

[‡]School of Materials Science and Engineering, Chongqing Jiaotong University, Chongqing 400074, China

[∥]Centre for Photonics Research, Guilin University of Electronic Technology, Guilin, 541004, China

[⊥]Laboratory of Weak Light Nonlinear Photonics Ministry of Education, School of Physics and Teda Applied Physics Institute, Nankai University, Tianjin 300071, China

Supporting Information

ABSTRACT: The depth of focus of an imaging system determines the range of change for both the position of focal plane and image plane. Although a typical light sword optical element with angular modulation of phase transmittance can extend its focus of depth due to its angular variation of the optical power, it lacks rotational symmetry and exhibits a junction, rendering its fabrication extremely difficult. Optical metasurfaces provide an unusual approach to develop such a device due to their unprecedented capability in the manipulation of light propagation in a desirable manner. We propose and experimentally demonstrate a light sword metasurface lens with multiple functionalities. The position of focal segments can be controlled by changing the polarization state of the incident light. The developed ultrathin, ultraflat device can facilitate device miniaturization and system integration and may find applications in various fields such as optical coupling, imaging, and interconnections.

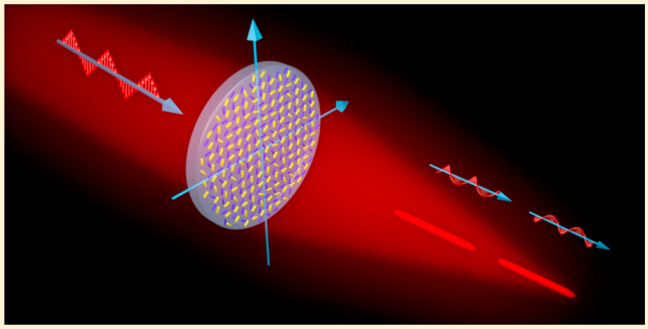

KEYWORDS: *metasurface, light sword lens, multiple functionalities, long focus of depth*

Depth of focus is one of important parameters for an imaging system, which determines the range of change for the position of focal plane and image plane. Extending depth of focus of lens has attracted much attention due to its practical applications. Various methods have been proposed to produce an optical element with long depth of focus, including Yang-Gu algorithm,[1] inverse quartic axicon,[2] and light sword optical element (LSOE).[3,4] In contrast to other solutions, LSOEs have demonstrated their superiority especially for multifocal imaging with extended depth of focus.[5] LSOEs are distinguished by angular variation of the optical power since every infinitesimal angular sector has its own focal length, leading to the independence of their optical power range with respect to the pupil's diameter. These devices are typically made by fabricating a transparent substrate at different depths to yield a desired phase profile in the transmitted light. However, LSOEs lack rotational symmetry and exhibit a junction, rendering their fabrication extremely difficult. For example, the surface curvature of such an element continuously and smoothly varies across the entire surface, which results in the discontinuity observed as a radially placed edge. There are technical challenges for manufacturing to accurately produce such a smooth, continuous surface with a sharp edge. Furthermore, the sharp edge may hinder its applications in system integration since it must be handled with extreme care, which increases the difficulty level for system assembly. Although diffractive optical elements have the advantage of being relatively flat, their fabrication process is not suitable for the light sword devices since they are highly susceptible to fabrication errors, especially at a point where a big phase change jump is required.

Optical metasurfaces, which are two-dimensional counterparts of metamaterials with subwavelength thickness, have aroused considerable interest since they can control light propagation in a desirable manner, providing a viable route to develop ultrathin, ultraflat optical devices.[6−15] Metasurfaces consist of a single layer or few-layer stacks of artificial planar structures and can engineer the amplitude, phase, and polarization of a light beam at subwavelength resolution, making them possible to solve the fabrication challenge in optical devices based on phase accumulation due to the propagation effect.[16−18] A plethora of applications on

Special Issue: Ultra-Capacity Metasurfaces with Low Dimension and High Efficiency

Received: December 14, 2017
Published: March 17, 2018

DOI: 10.1021/acsphotonics.7b01536
ACS Photonics 2018, 5, 1794−1799

metasurfaces have been proposed and demonstrated, such as beam shaper,[19] orbital angular momentum manipulation,[20,21] ultrathin metalenses,[17,22] spin Hall effect of light,[23] and optical holography.[8,11,13,24] To tackle the technical fabrication challenge in LSOEs, we propose and experimentally demonstrate a facile metasurface approach to develop multifunctional light sword metasurface lenses (MLSMLs). In comparison with traditional bulky LSOEs with wavelength-dependent phase profile based on optical path difference, the developed MLSMLs are ultrathin, ultraflat and ideal for device miniaturization and system integration. Although using optical metasurfaces to design polarization-controlled lens with needle-shaped focal points has been theoretically proposed,[25] it has not been experimentally demonstrated. Furthermore, unlike previously demonstrated LSOEs, the functionality of the fabricated device here can be changed by controlling the polarization state of the incident light. Our demonstrated results might enable new types of ultracompact optical elements for generating LSOEs with long focus of depth and also advance metasurface-based multifunctional devices.

DESIGN AND METHODS

Figure 1 shows the schematic of the MLSML when illuminated by a linearly polarized light beam at normal incidence. The

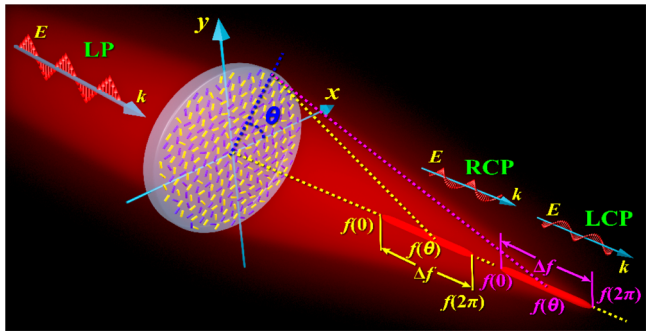

Figure 1. Schematic of multifunctional light sword metasurface lens. Each infinitesimal angular sector is equivalent to a Fresnel lens with a focal length $f + \Delta f\theta/2\pi$, where f, Δf, and θ represent focal length, focal range and azimuthal coordinate, respectively. Upon the illumination of an incident light with linear polarization (LP), the device has two real focal segments corresponding to the transmitted light with right circular polarization (RCP) and left circular polarization (LCP). The metasurface consists of gold nanorods with spatially varying orientation.

unique metasurface device here functions as a combination of two separate LSOEs since it has two different focal lengths with same focal range (Δf) for circularly polarized light with opposite helicity (left-handed and right-handed circular polarizations, LCP and RCP). Each infinitesimal angular sector on the individual device is equivalent to a Fresnel lens with a focal length $f + \Delta f\theta/2\pi$, where θ is the azimuthal angle. A circularly polarized light beam can be focused into one of focal segments stretched from f up to $f + \Delta f$ by such an optical element. The two separate focal segments correspond to the incident light with different circular polarizations. Upon the illumination of a linearly polarized light beam, two focal segments are obtained since it can be decomposed into LCP light and RCP light with same components. Thus, the focal segments of the designed device can be changed by controlling the polarization state of the incident light. To achieve the desired phase profile while maintaining uniform amplitude, a metasurface consisting of gold nanorods with spatially variant orientations is used. When an incident circularly polarized beam normally passes through the anisotropic nanorods, the transmitted beam contains both the original spin part without phase shift and the converted spin part with the induced phase shift (known as Pancharatnam-Berry phase). The additional phase delay is $\pm 2\varphi$ (φ is the orientation angle of nanorod) for the cross-polarization (RCP/LCP) transmitted waves, where the plus/minus sign is decided by the helicity of the incident light.[17]

The phase transmittance of the MLSML is defined by the following relation:[26,27]

$$\varphi(r, \theta) = \pm \frac{kr^2}{2[f + (\Delta f\theta/2\pi)]} \quad (1)$$

where r,θ are the radial and azimuthal coordinate, respectively. The angle θ ranges from 0 to 2π. $k = 2\pi/\lambda$ is the free-space wave vector, and λ is the wavelength of the incident light. The parameters f and Δf represent the focal length and the focal range of the element, respectively. From the eq 1, we can see that each infinitesimal angular sector is equivalent to a Fresnel lens with a focal length $f + \Delta f\theta/2\pi$. Therefore, the LSOE-based metasurface lens can focus approximately a plane wave into a focal segment stretched from f up to $f + \Delta f$. Note that the "+" and "−" signs in eq 1 correspond to a positive (convex) and negative (concave) polarity, respectively, for the incident LCP and RCP light. To design such a multifunctional device, two metasurfaces (each one for a specific focal segment) are designed to operate with opposite incident helicities and merged together with a displacement. Suppose d_1 is the distance between neighboring nanorods with a value of 424 nm along both x and y directions, the displacement vector is $(d_1/2, d_1/2)$, as detailed in Figure 2. Each gold nanorod is 200 nm long, 70 nm wide, and 40 nm thick. There are two separate metasurfaces that can generate two different types of required phase profiles, but the size of the sample before and after metasurface merging is the same and the equivalent pixel size in the merged metasurface is 300 nm × 300 nm. Indium−tin-oxide (ITO)-coated glass substrates are used to fabricate the designed nanorod structures. Nanostructures are defined in a positive PMMA resist film on glass substrates using standard electron-beam lithography. Then a 40 nm gold film is deposited on the sample via electron beam evaporation. Finally, the metasurface consisting of gold nanorods is achieved by a subsequent lift-off procedure. Figure 2f shows the scanning electron microscopy (SEM) image of part of our fabricated multifunctional device. Figure 2c, d, and g are the magnified figures for the regions A, B, and C, respectively. Figure 2c,d clearly shows the phase-edge of our light sword metasurface lens (similar to traditional light sword lenses).

RESULTS AND DISCUSSIONS

Under the illumination of LCP light and RCP light at normal incidence, the simulation and experimental results for light focusing with long focus of depth at the wavelength of 650 nm are shown in Figure 3. The converted part with phase change is characterized by filtering out the nonconverted part in our experiment. The focal lengths for LCP and RCP light are chosen to be 1400 and 1500 μm, respectively. However, their focal range Δf is the same (50 μm). To generate two LSOEs with different polarity for the same circular polarization (e.g., LCP), the signs of the phase profile for the two optical

DOI: 10.1021/acsphotonics.7b01536
ACS Photonics 2018, 5, 1794−1799

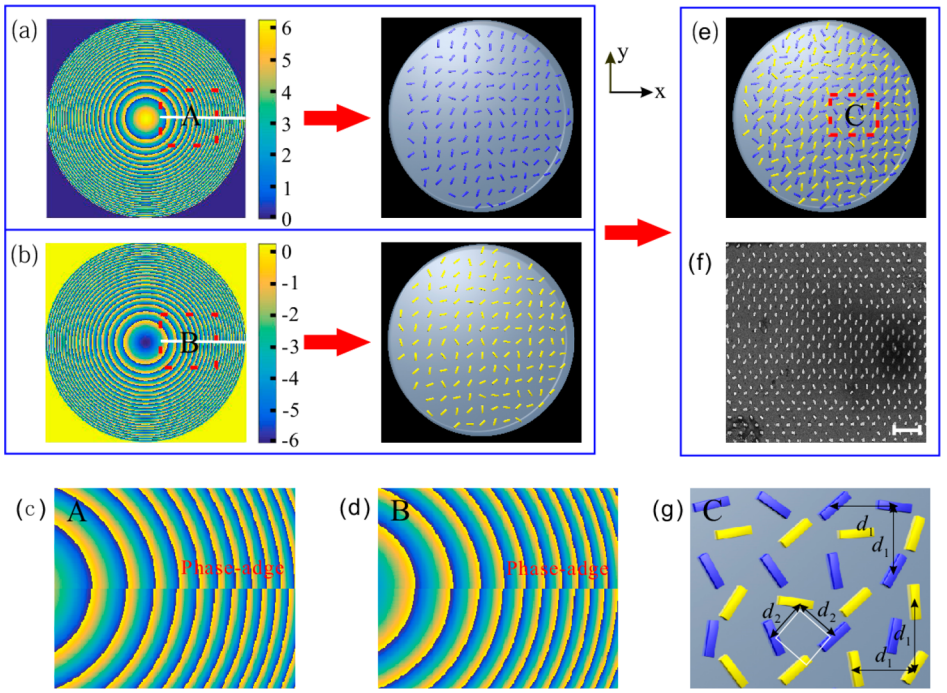

Figure 2. Generation of the multifunctional light sword metasurface lens and scanning electron microscopy (SEM) image of the sample. Suppose d_1 is the distance between neighboring antennas with a value of 424 nm along x and y directions. Two sets of light sword metasurface lenses are designed to operate with opposite incident helicities and merged together with a displacement vector of $(d_1/2, d_1/2)$. d_2 is the equivalent distance between neighboring nanorods in the merged metasurface, which is 300 nm. Upon the illumination of LCP light at normal incidence, the signs of generated phase profiles for the transmitted lights beams are (a) positive and (b) negative, respectively. (e) Schematic of the merged metasurface. (f) SEM image of part of the multifunctional metasurface lens. The scale bar is 1 μm. (c and d) Phase distributions in the regions of A and B marked by the dotted rectangles, respectively. (g) Nanorod distribution in the region C.

elements are chosen to be "+" and "−", respectively (as shown in eq 1). Therefore, only one real focal segment is expected when an incident light beam with pure circular polarization (LCP or RCP) shines on the sample. To further analyze the characteristic of long focus depth, the light intensity distributions along the longitudinal direction at the positions of 1375, 1400, and 1425 μm (marked by regions I−III) are also given in Figure 3a. The three focal spots in the transverse plane unambiguously show that the designed device has a long focus of depth. Similarly, another real focal segment is predicted if the polarization state of the incident light is changed from LCP to RCP. The light intensity distributions along the longitudinal direction at the positions of at the location of 1475, 1500, and 1525 μm (marked by IV−VI) are also given (see Figure 3b). The experimental setup to characterize the fabricated metasurface device is shown in Figure S1 (Supporting Information). The sample is mounted on a 3D translation stage, allowing for fine adjustment. The incident light at the wavelength of 650 nm is from a tunable supercontinuum laser source (NKT-SuperK EXTREME). The required polarization state is generated by a polarizer and a quarter-wave plate. Since the sign of the phase profile can be flipped by controlling the helicity of the incident light, the focal segments will be swapped along the longitudinal direction when the helicity of the incident light is changed from LCP to RCP (shown in Figure 3b). The full width at half-maximum (fwhm) is an important parameter commonly used to describe the spot size of a focal point. The simulated fwhm's for the three real focal points in regions I−III in Figure 3a are 3.6, 4.2, and 4.2 μm, respectively. In contrast, the experimental measured fwhm's are 5.7, 6.03, and 6.03 μm, respectively. The measured fwhm's for IV, V, and VI are that 5.03, 4.2, and 6.7 μm, respectively, while the corresponding simulated values are 4, 4.2, and 4.4 μm, respectively. The deviation is mainly due to the fabrication error and measurement accuracy. Nevertheless, good agreement between simulation and experiment is found.

We further characterize the performance of the developed device for the incident light with linear polarization. Figure 4b shows the experimentally measured intensity distributions at six longitudinal positions marked by I−VI, corresponding to 1375, 1400, 1425, 1475, 1500, and 1525 μm, respectively. The regions I−III belong to the first focal segment and the regions IV−VI belong to the second one, as shown in Figure 4a. Their light intensity distributions have similar tendency as shown in Figure 3a,b except for the regions III and IV. The light intensities in region III and IV shown in Figure 4b are stronger than those in Figure 3a,b, which is due to the fact that the distance between the two focal segments is relatively close and results in intensity overlap in these regions.

The conversion efficiency between the two circular polarization states is an important parameter in the performance of the metasurface device. This value is defined as the ratio of the power of the helicity-changed light (e.g., from LCP to RCP or RCP to LCP) to that of the input light. It is worth mentioning that the efficiency of the device is halved since a linearly polarized light beam can be decomposed into two circularly polarized lights beams with opposite helicity. As a proof-of-concept, the conversion efficiency between the polarization states based on the plasmonic metasurface is measured to be 2% at 650 nm, which is at the lower edge of what is required for practical applications. As an alternative to metallic nanorods, however, a dielectric metasurface can be used to dramatically increase this value since it can decrease the ohmic losses and

DOI: 10.1021/acsphotonics.7b01536
ACS Photonics 2018, 5, 1794−1799

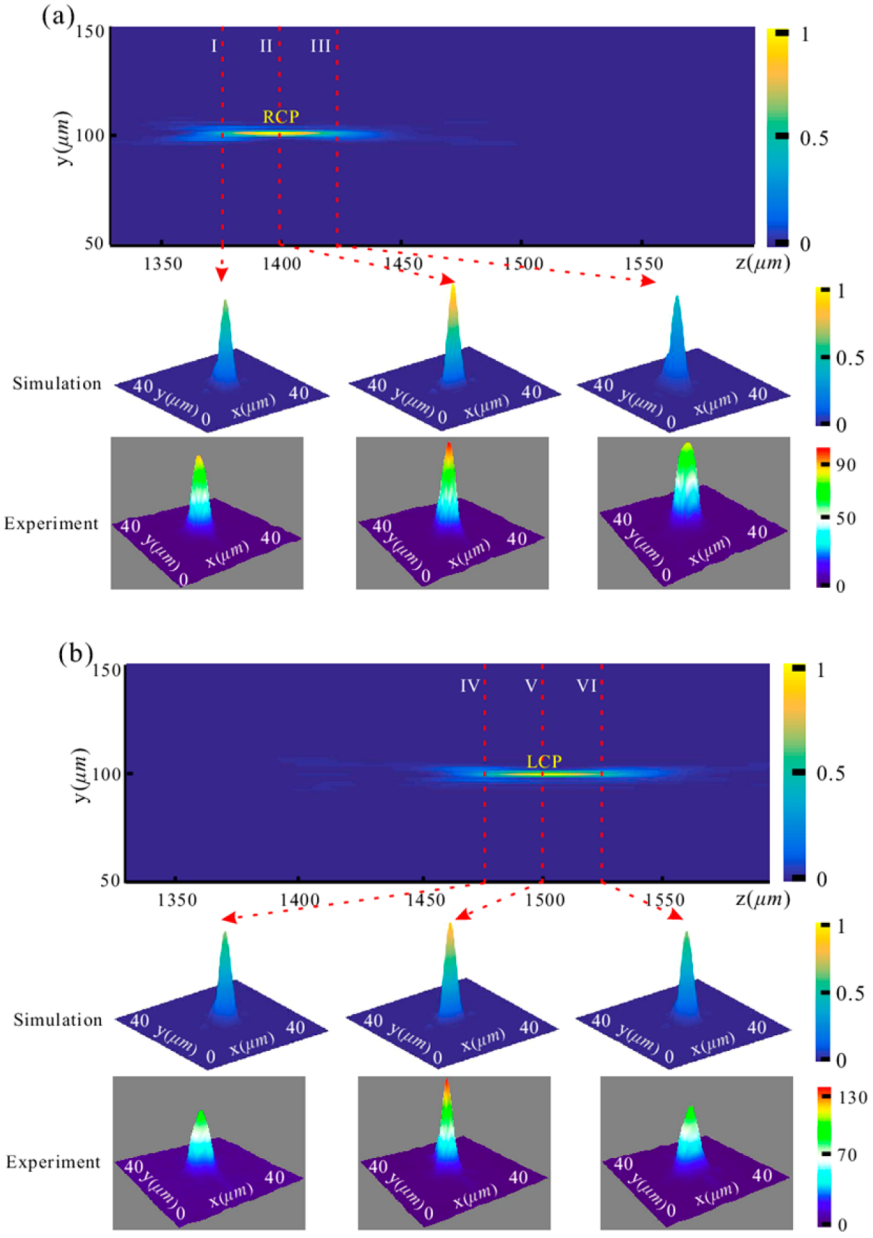

Figure 3. Simulation and experimental results of the multifunctional metasurface device at 650 nm. (a) The focusing performance of the metasurface lens when illuminated by an incident light with left circular polarization (LCP) at normal incidence. Theoretical and measured intensity distributions in the three focal planes located at longitudinal positions of 1375, 1400, and 1425 μm (marked by regions I–III) are also given. (b) Simulation and experimental results for the incident light with right circular polarization (RCP).

improve the scattering cross sections of the metal nanorods.[28,29]

An interesting question is whether there is a limit in the depth of focus in this design. Each infinitesimal angular sector on the metasurface device is equivalent to a Fresnel lens with a specific focal length. With the increase of the depth of focus, the phase difference between unit cells will be insufficient, leading to the decrease of energy in each focal plane along the longitudinal direction within the depth of focus. Furthermore, the background noise will increase and the contrast will become worse. Our design is based on transmission mode, while Veysi's work is based on reflective operation,[25] which is not compatible with most optical systems that operate in the transmission mode. In addition, the multiple functionality in our work is realized by controlling circular polarization of the incident light, instead of linear polarization in Veysi's work. Furthermore, in comparison with Y-shaped structures proposed by Veysi, nanorod structures are much simpler, which can facilitate nanofabrication.

CONCLUSION

In conclusion, we have theoretically and experimentally demonstrated a facile metasurface approach to realize a light sword lens with multiple functionalities based on the geometric design and arrangement of light-scattering nanoantennas. The desired phase profile is realized by a metasurface consisting of nanorods with spatially variant orientation. The functionality of the fabricated ultrathin, flat light sword metasurface device can be controlled by changing the polarization state of the incident light, which enables the realization of novel optical components

DOI: 10.1021/acsphotonics.7b01536
ACS Photonics 2018, 5, 1794–1799

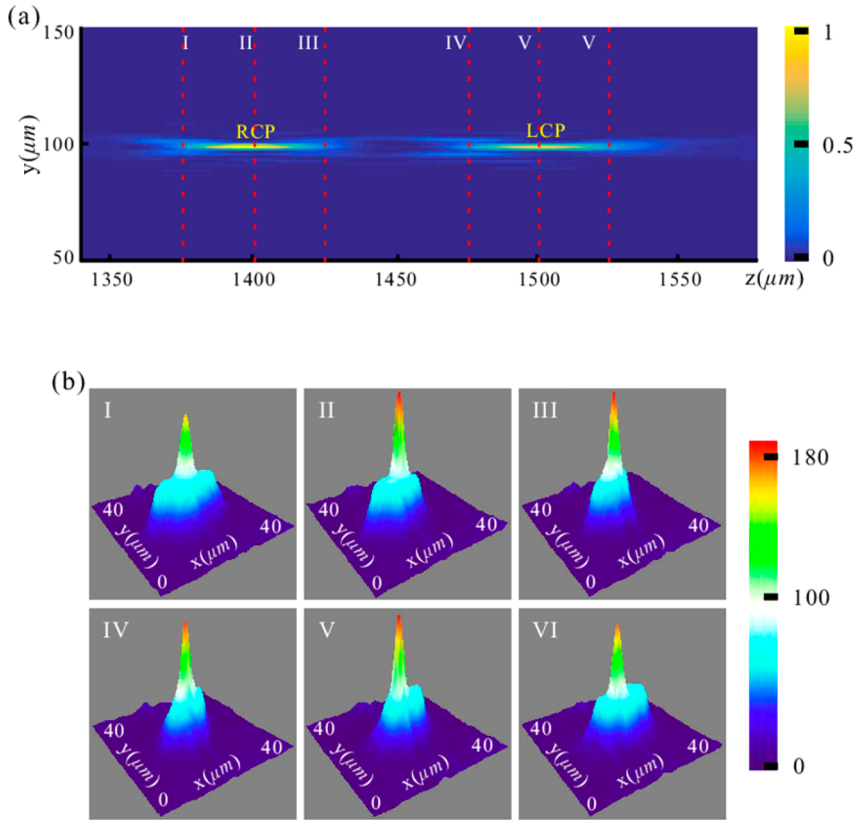

Figure 4. Simulation and experimentally measured results for the incident light with linear polarization. (a) Two focal segments for light with different helicities are observed in the simulation since a linearly polarized light can be decomposed into a LCP light beam and a RCP light beam with same components. (b) Experimentally measured intensity distributions in the focal planes located at six longitudinal positions.

with functionalities tailored to specific applications. The fabrication procedure is compatible with standard semiconductor fabrication process and the compact device can facilitate device miniaturization and system integration, which may find applications in optical coupling, imaging, and interconnections.

■ ASSOCIATED CONTENT

Supporting Information

The Supporting Information is available free of charge on the ACS Publications website at DOI: 10.1021/acsphotonics.7b01536.

Supporting Figure S1 (PDF).

■ AUTHOR INFORMATION

Corresponding Author

*E-mail: x.chen@hw.ac.uk.

ORCID

Shuqi Chen: 0000-0002-7898-4148

Xianzhong Chen: 0000-0001-7521-1548

Author Contributions

§These authors contributed equally to this work.

Notes

The authors declare no competing financial interest.

■ ACKNOWLEDGMENTS

X.C. acknowledges the Engineering and Physical Sciences Research Council of the United Kingdom (Grant ref: EP/P029892/1). Z.Z. would like to acknowledge National Natural Science Foundation of China (Grant No. 11504034), Chongqing Research Program of Basic Research and Frontier Technology (Grant No. cstc2016jcyjA0186), and financial support from the China Scholarship Council (Grant No. 201608500036).

■ REFERENCES

(1) Dong, B. Z.; Yang, G. Z.; Gu, B. Y.; Ersoy, O. K. Iterative optimization approach for designing an axicon with long focal depth and high transverse resolution. *J. Opt. Soc. Am. A* **1996**, *13*, 97−103.

(2) Ares, J.; Flores, R.; Bará, S.; Jaroszewicz, Z. Presbyopia compensation with a quartic axicon. *Optom. Vis. Sci.* **2005**, *82*, 1071−1078.

(3) Petelczyc, K.; Bará, S.; Lopez, A. C.; Jaroszewicz, Z.; Kakarenko, K.; Kolodziejczyk, A.; Sypek, M. Imaging properties of the light sword optical element used as a contact lens in a presbyopic eye model. *Opt. Express* **2011**, *19*, 25602−25616.

(4) Kołodziejczyk, A.; Bará, S.; Jaroszewicz, Z.; Sypek, M. The light sword optical element—a new diffraction structure with extended depth of focus. *J. Mod. Opt.* **1990**, *37*, 1283−1286.

(5) Kakarenko, K.; Ducin, I.; Grabowiecki, K.; Jaroszewicz, Z.; Kolodziejczyk, A.; Mira-Agudelo, A.; Petelczyc, K.; Składowska, A.; Sypek, M. Assessment of imaging with extended depth-of-field by means of the light sword lens in terms of visual acuity scale. *Biomed. Opt. Express* **2015**, *6*, 1738−1748.

(6) Yu, N.; Genevet, P.; Kats, M. A.; Aieta, F.; Tetienne, J. P.; Capasso, F.; Gaburro, Z. Light propagation with phase discontinuities: generalized laws of reflection and refraction. *Science* **2011**, *334*, 333−337.

(7) Huang, L.; Chen, X.; Mühlenbernd, H.; Li, G.; Bai, B.; Tan, Q.; Jin, G.; Zentgraf, T.; Zhang, S. Dispersionless phase discontinuities for controlling light propagation. *Nano Lett.* **2012**, *12*, 5750−5755.

DOI: 10.1021/acsphotonics.7b01536
ACS Photonics 2018, 5, 1794−1799

(8) Zheng, G.; Mühlenbernd, H.; Kenney, M.; Li, G.; Zentgraf, T.; Zhang, S. Metasurface holograms reaching 80% efficiency. *Nat. Nanotechnol.* **2015**, *10*, 308−312.
(9) Ni, X.; Wong, Z. J.; Mrejen, M.; Wang, Y.; Zhang, X. An ultrathin invisibility skin cloak for visible light. *Science* **2015**, *349*, 1310−1314.
(10) Genevet, P.; Capasso, F.; Aieta, F.; Khorasaninejad, M.; Devlin, R. Recent advances in planar optics: from plasmonic to dielectric metasurfaces. *Optica* **2017**, *4*, 139−152.
(11) Chen, W. T.; Yang, K. Y.; Wang, C. M.; Huang, Y. W.; Sun, G.; Chiang, I. D.; Liao, C. Y.; Hsu, W. L.; Lin, H. T.; Sun, S.; Zhou, L. High-efficiency broadband meta-hologram with polarization-controlled dual images. *Nano Lett.* **2014**, *14*, 225−230.
(12) Sun, S.; He, Q.; Xiao, S.; Xu, Q.; Li, X.; Zhou, L. Gradient-index meta-surfaces as a bridge linking propagating waves and surface waves. *Nat. Mater.* **2012**, *11*, 426−431.
(13) Hu, D.; Wang, X.; Feng, S.; Ye, J.; Sun, W.; Kan, Q.; Klar, P. J.; Zhang, Y. Ultrathin terahertz planar elements. *Adv. Opt. Mater.* **2013**, *1*, 186−191.
(14) Li, J.; Chen, S.; Yang, H.; Li, J.; Yu, P.; Cheng, H.; Gu, C.; Chen, H. T.; Tian, J. Simultaneous control of light polarization and phase distributions using plasmonic metasurfaces. *Adv. Funct. Mater.* **2015**, *25*, 704−710.
(15) Liu, L.; Zhang, X.; Kenney, M.; Su, X.; Xu, N.; Ouyang, C.; Shi, Y.; Han, J.; Zhang, W.; Zhang, S. Broadband metasurfaces with simultaneous control of phase and amplitude. *Adv. Mater.* **2014**, *26*, 5031−5036.
(16) Li, G.; Zhang, S.; Zentgraf, T. Nonlinear photonic metasurfaces. *Nat. Rev. Mater.* **2017**, *2*, 17010.
(17) Chen, X.; Huang, L.; Mühlenbernd, H.; Li, G.; Bai, B.; Tan, Q.; Jin, G.; Qiu, C.; Zhang, S.; Zentgraf, T. Dual-polarity plasmonic metalens for visible light. *Nat. Commun.* **2012**, *3*, 1198.
(18) Wen, D.; Yue, F.; Li, G.; Zheng, G.; Chan, K.; Chen, S.; Chen, M.; King Fai Li, K. F.; Wong, P. W. H.; Cheah, K. W.; Pun, E. Y. B.; Zhang, S.; Chen, X. Helicity multiplexed broadband metasurface holograms. *Nat. Commun.* **2015**, *6*, 8241.
(19) Chen, X.; Zhang, Y.; Huang, L.; Zhang, S. Ultrathin metasurface laser beam shaper. *Adv. Opt. Mater.* **2014**, *2*, 978−982.
(20) Yue, F.; Wen, D.; Zhang, C.; Gerardot, B. D.; Wang, W.; Zhang, S.; Chen, X. Multichannel Polarization-Controllable Superpositions of Orbital Angular Momentum States. *Adv. Mater.* **2017**, *29*, 1603838.
(21) Ma, X.; Pu, M.; Li, X.; Huang, C.; Wang, Y.; Pan, W.; Zhao, B.; Cui, J.; Wang, C.; Zhao, Z.; Luo, X. A planar chiral meta-surface for optical vortex generation and focusing. *Sci. Rep.* **2015**, *5*, 10365.
(22) Aieta, F.; Genevet, P.; Kats, M. A.; Yu, N.; Blanchard, R.; Gaburro, Z.; Capasso, F. Aberration-free ultrathin flat lenses and axicons at telecom wavelengths based on plasmonic metasurfaces. *Nano Lett.* **2012**, *12*, 4932−4936.
(23) Yin, X.; Ye, Z.; Rho, J.; Wang, Y.; Zhang, X. Photonic spin Hall effect at metasurfaces. *Science* **2013**, *339*, 1405−1407.
(24) Larouche, S.; Tsai, Y. J.; Tyler, T.; Jokerst, N. M.; Smith, D. R. Infrared metamaterial phase holograms. *Nat. Mater.* **2012**, *11*, 450−454.
(25) Veysi, M.; Guclu, C.; Boyraz, O.; Capolino, F. Reflective metasurface lens with an elongated needle-shaped focus. *J. Opt. Soc. Am. B* **2017**, *34*, 374−382.
(26) Petelczyc, K.; Garcia, J. A.; Bara, S.; Jaroszewicz, Z.; Kakarenko, K.; Kolodziejczyk, A.; Sypek, M. Strehl ratios characterizing optical elements designed for presbyopia compensation. *Opt. Express* **2011**, *19*, 8693−8699.
(27) Petelczyc, K.; Garcia, J. A.; Bará, S.; Jaroszewicz, Z.; Kołodziejczyk, A.; Sypek, M. Presbyopia compensation with a light sword optical element of a variable diameter. *Photonics Letters of Poland* **2009**, *1*, 55−57.
(28) Khorasaninejad, M.; Chen, W. T.; Devlin, R. C.; Oh, J.; Zhu, A. Y.; Capasso, F. Metalenses at visible wavelengths: Diffraction-limited focusing and subwavelength resolution imaging. *Science* **2016**, *352*, 1190−1194.
(29) Arbabi, A.; Horie, Y.; Bagheri, M.; Faraon, A. Dielectric metasurfaces for complete control of phase and polarization with subwavelength spatial resolution and high transmission. *Nat. Nanotechnol.* **2015**, *10*, 937−943.

DOI: 10.1021/acsphotonics.7b01536
ACS Photonics 2018, 5, 1794−1799